Terahertz Modulator Based on Vertically Coupled Fano Metamaterial

Tuan Anh Pham Tran and Peter Haring Bolívar, *Member, IEEE*

***Abstract*—We introduce a vertical coupling concept to Fano resonance based terahertz (THz) metamaterials, in order to enhance their modulation characteristics. The approach is demonstrated for an asymmetric split-ring structure fabricated from gold with standard micromachining processes on a fused silica substrate. The realized samples are characterized with THz time-domain spectroscopy and the results are in close agreement with the simulation model. Due to the enhanced field concentration facilitated by vertical coupling, we achieve a 95% modulation depth and 35% resonance frequency tunability at 1.23 THz with less than 1-dB inherent loss. The exemplary device shows vertical coupling as an attractive concept for designing efficient modulators for terahertz imaging applications.**

***Index Terms*—Intensity modulation, submillimeter wave filters, submillimeter wave measurements, terahertz imaging, terahertz metamaterials, terahertz modulators, tunable circuits and devices.**

I. Introduction

SINCE the seminal paper of Pendry [1], studies on metamaterials, periodic subwavelength structures that exhibit engineerable electromagnetic properties [2], have come a long way from simple passive micro- and nanostructures to actively reconfigurable devices [3]–[5]. While in established areas of the electromagnetic spectrum, such as microwaves and optical frequencies, the impact of this new class of material is not yet extensive. Metamaterial research and device developments thrive to solve existing application hindrances in the terahertz frequency regime. The lack of adequate materials and devices operating in this area of electromagnetic spectrum and the compatibility of metamaterial structure size to the established microfabrication techniques have made metamaterial an ideal candidate to fill the "terahertz technological gap" [6]–[8].

Many applications in terahertz technology require control elements that modulate the amplitude and/or phase of a terahertz beam. One particularly interesting component is spatially addressable modulator necessitated in imaging or beamforming applications. During the past several years, with the intensive research on metamaterials operating in terahertz frequency range, many novel dynamically tunable metamaterial devices have been proposed [3], [9]. Among different strategies to alter/tune the response of metamaterials, the most promising techniques that can be applied to arrays with independently switchable pixels are carrier depletion at Schottky contacts [10], [11], liquid crystals [12], and microelectromechanical systems (MEMS) based devices [13], [14].

Proposed modulator structures are mainly based on altering the capacitance of the element or the capacitive coupling between elements, either by modifying the property of the dielectric or changing the distance between the electrodes. However most of these tuning elements, which are always embedded into a particularly sensitive coupling section of the metamaterial, are based on planar structures, which are simple to fabricate, but also unavoidably means that the tuning capacitance of the device mainly results from thin, laterally coupling structures (e.g., metalization side walls or thin depletion layers with less than 1-μm thickness). This inevitably leads to small capacitance and low tunability range, as it can exemplarily be seen in the design of Chen *et al.* [10], which has a small resonance shift and only 3-dB modulation depth (MD). By changing such lateral concepts to *vertical* coupling, a significantly higher tunability performance can be achieved. Up to now, only one vertically tuned THz modulator has been proposed: a microfabricated structure by Han *et al.* [14] demonstrated a markedly enhanced resonance shift of 45% and MD of more than 16 dB. However, this design still relies on tuning a conventional dipole resonance, which is not sensitive and hence requires a bulky actuator structure. Here, we demonstrate a vertically coupled Fano resonance as an attractive approach to enhance the characteristics of THz metamaterial based modulators.

The concept of Fano resonance [15] was introduced to the field of THz metamaterials to realize high Q-factor devices [16], [17], which is particularly problematic in the THz frequency range, given the comparatively high dielectric loss in this domain. Relying only on the constructive and destructive interferences of different electromagnetic eigenmodes, e.g., in asymmetric double dipole microstructures, this resonance type is very sensitive to a minute change in the geometric conformation of material dielectric properties of tuning elements. One particular structure that possessed a strong Fano resonance due to coherent excitations of metamolecules is the asymmetric double split ring [18], which leads to the development of ultrasensitive chemical or biological sensors [19]. The Q-factor of the resonance can also be engineered by altering the asymmetry [20]. Nevertheless, as elucidated above, all the state-of-the-art

Manuscript received March 16, 2018; revised June 11, 2018; accepted June 19, 2018. Date of publication July 13, 2018; date of current version September 10, 2018. This work was supported by the DFG Research Training Group 1564 (GRK). *(Corresponding author: Tuan Anh Pham Tran.)*

The authors are with the Institute for High Frequency and Quantum Electronics, School of Science and Technology, University of Siegen, Siegen D-57076, Germany (e-mail: tuananh.phamtran@uni-siegen.de; peter.haring@uni-siegen.de).

Color versions of one or more of the figures in this paper are available online at http://ieeexplore.ieee.org.

Digital Object Identifier 10.1109/TTHZ.2018.2851919

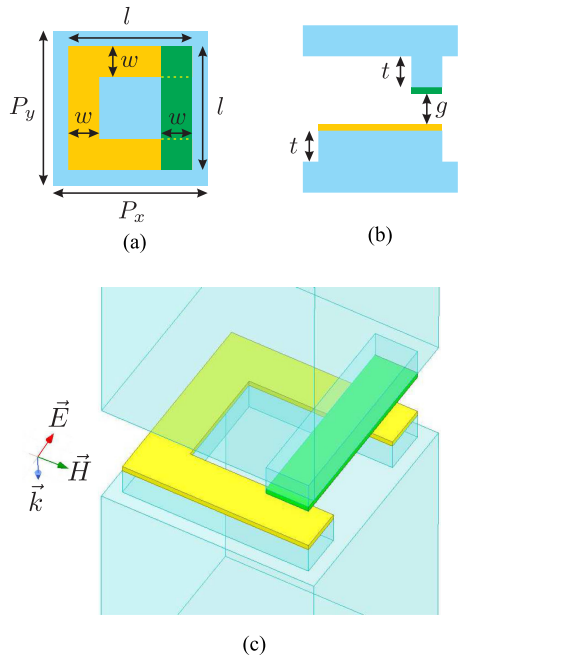

Fig. 1. (a) Top view, (b) cross-sectional view, and (c) three-dimensional view of the unit cell of the vertically coupled double split-ring resonator structure. Drawing is not to scale.

designs exhibit low modulation contrast and have high insertion losses that are detrimental to modulator applications, given the planar nature and lateral coupling of existing concepts. Our approach builds upon a vertical gap asymmetric double split-ring resonator, as suggested earlier [21] for static detectors and gain medium.

In this paper, we demonstrate the excellent potential of such a vertical metamaterial structure for THz modulator applications. With our design the gaps' capacitance alteration is greatly enhanced in comparison with planar Fano structures, as shown in both simulation and experiment. The proof-of-concept demonstrator achieves up to 95% MD at 1.23 THz and 35% resonance frequency shift. Our results exhibit great potential to fabricate a focal plane array modulator for THz imaging and beam steering applications.

II. Structure Modeling, Sample Fabrication, and Measurement Setup

A. Structure Design and Simulation

The unit cell of the metamaterial is illustrated in Fig. 1. The structure consists of two parts, which are the two halves of the square split ring on a fused silica substrate. The period is $P = P_x = P_y = 50\,\mu$m, the ring sides are $l = 40\,\mu$m long, and the width of the ring is $w = 10\,\mu$m. The glass substrate is etched down with an etch depth $t = 5\,\mu$m for the complete area, except under the ring parts. The vertical gap of the double split ring g is varied between 1 and 10 μm as this range of actuation is compatible with MEMS integration technologies. The split-ring material is of gold with 100-nm thickness and conductivity 4.1×10^7 S·m^{-1}. Fused silica is modeled as a lossy material with dielectric constant $\epsilon = 3.78$ [25] and loss tangent of 0.01, which

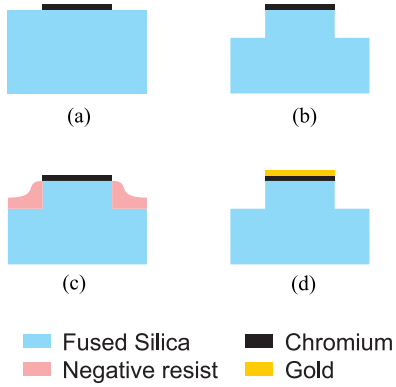

Fig. 2. Fabrication steps. (a) Pattern chromium structure. (b) Reactive ion etching (RIE) of a fused silica substrate. (c) Spin-coat negative resist and back-side exposure. (d) Sputter gold and lift off.

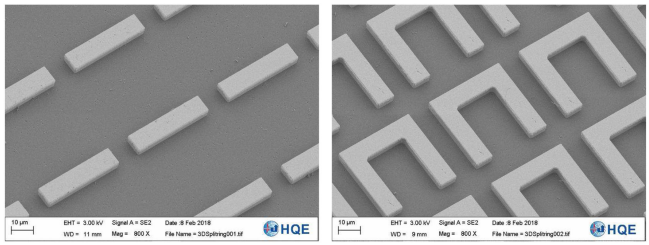

Fig. 3. SEM images of the fabricated demonstrator. The two parts of the double split-ring array were structured on 1-mm-thick fused silica substrate and had 100/100 nm gold/chromium metalization.

is a worst case estimation of the spectrally resolved measured values.

We modeled and simulated the metamaterial structure using commercially available Maxwell's equation solver HFSS from ANSYS. The boundary conditions are periodic types and the excitation sources are Floquet ports. The magnitudes of the complex transmittances S_{21} are used to compare with experimental transmission data. The field for normalization is computed inside the glass substrate so that the results are the response of this metamaterial alone (i.e., no reflection loss from the substrate.)

B. Fabrication

The two parts of the double split ring had identical processing steps and were fabricated on the same wafer as sketched in Fig. 2. First, the 1-mm-thick fused silica substrate was patterned with 200-nm chrome structures, which was used as a mask for RIE step having an etch depth of 5 μm. After etching around 100 nm of chrome remains, which was thick enough to be used as mask for optical lithography, the wafer was then spin coated with 2-μm negative resist and exposed to UV light from the back side. After development, 100 nm of gold was deposited and a lift-off step was used to obtain the final chrome/gold structure. Fig. 3 shows the SEM images of the two halves of the fabricated metamaterial. The total metamaterial area is 8×8 mm^2.

C. Measurement Setup and Methods

Our THz time-domain spectrometer (TDS) setup is shown schematically in Fig. 4. The GaAs photoconductive emitter was

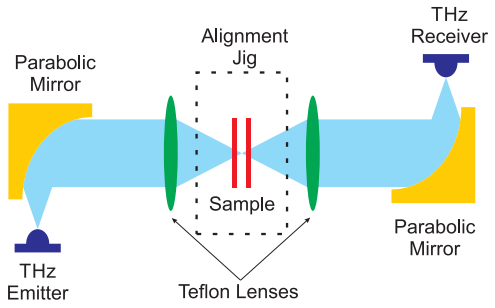

Fig. 4. Schematic diagram of the THz time-domain spectroscopy setup. THz radiation was generated with a photoconductive antenna and detected with an electro-optical sampling technique. Beam routing was done using two off-axis parabolic mirrors and two focusing teflon lenses. The two parts of the double split-ring sample were mounted on an alignment fixture that was inserted between the two lenses. We used an optical microscope to facilitate the alignment and measure the gap distance. During THz spectroscopy measurements, the microscope was removed. The whole setup was enclosed in a nitrogen-purged box.

pumped by a commercial Ti:sapphire laser (femtolasers integral 20 HP) with 20-fs pulse at center wavelength of 800 nm and mean output of 300 mW. We used an electro-optic detection scheme with a 0.5-mm-long ZnTe crystal followed by a Wollaston prism and a pair of photodiodes. The THz beam was routed by two paraboloidal mirrors and focused using two teflon lenses. The THz focus spot diameter (10%–90% intensity) measured with a knife-edge method [22] was approximately 2 mm at 500 GHz, much smaller than the 8×8 mm^2 split-ring array area to avoid the boundary effect and to ease alignment.

In order to investigate the transmission characteristic of the metamaterial depending on its gap distance, we constructed a 6-DOF alignment fixture to hold the two halves of the sample. A motorized optical microscope was used for both alignment and surface separation measurement. The distance measurement method has an uncertainty of $\pm$ 0.5 μm and calibration was done by using reference samples measured with a Nikon confocal microscope with 40$\times$/0.6 NA objective. After the four corners of the sample (distance of 10 mm) were brought to the same separation within $\pm$1 μm and the absolute gap length in the center of the double split-ring array was noted, the microscope was removed to enable THz TDS measurement. From here, the gap distance was inferred from the initial value and the translation stage (VP-25XL from Newport) position, which has an accuracy of $\pm$0.5 μm. For normalization and insertion loss calculation, we measured also the system response without the sample and with the unstructured portion of the sample, which approximates two parallel 1-mm fused silica slabs with 10-μm separation.

III. Results and Discussion

A. Simulation Result and Analysis

The resulting transmission spectra for different gap distances are shown in Fig. 5, focusing on only the lowest order resonances. From the data, we can expect very low loss from the metamaterial alone outside the resonance area (less than 1 dB).

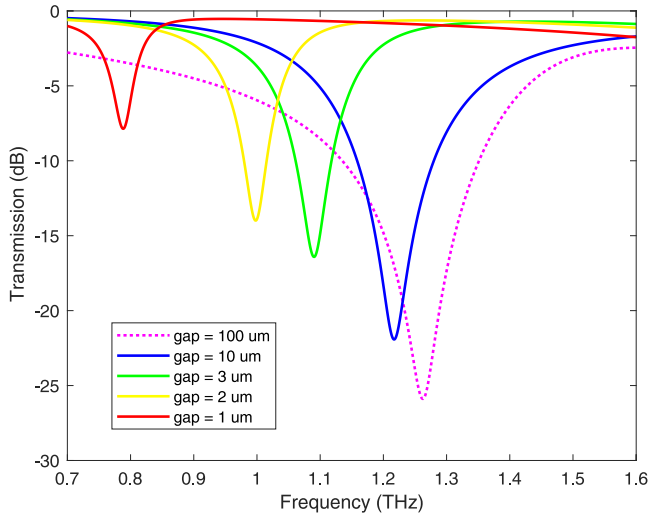

(a)

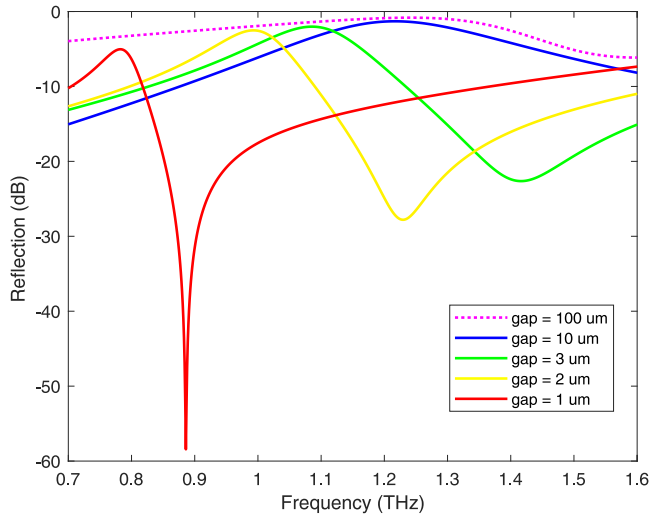

(b)

Fig. 5. (a) Simulated transmission spectra for different gap distances. The resonance frequency for gap of 1, 2, 3, 10, and 100 μm is 0.777, 1, 1.084, 1.214, and 1.257 THz and the Q-factor is 27, 39, 43, 52, and 50, respectively. (b) Corresponding reflection spectra.

The Q-factors Q s, which are defined as

$$Q = \frac{f_r}{\Delta f} \tag{1}$$

where f_r is the resonance frequency and Δf is the full width at half maximum, of the resonances are relatively high (40–50 except for 1-μm gap structure). It should be noted that we designed the resonator only for low loss and we can also tune the split-ring parameters to facilitate higher Q-factor structure [23]. Resonance shifts are expected to be very high (more than 400 GHz or 30%), and in per μm basis, the shift is greater when the gap is smaller, which clearly shows the capacitive loading effect. However, the resonance strength is also lower and the capacitive loading is higher. Hence, for a modulator application, we have a tradeoff between speed and contrast. For maximum contrast, we can choose the working point at larger gap and

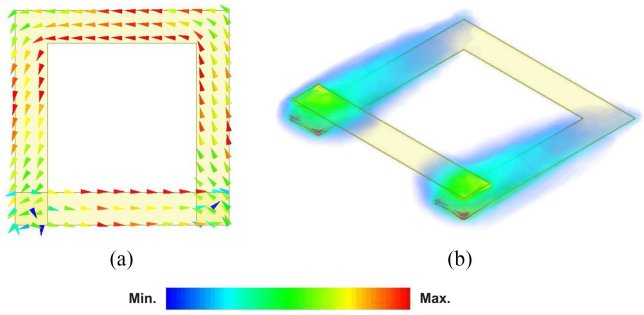

Fig. 6. (a) Simulated surface current and (b) electric-field distributions at the Fano resonance frequency of the structure with 4-μm gap distance.

actuate greater distance (e.g., between 10- and 3-μm gap to have more than 20-dB contrast), whereas for a fast modulation rate, we should stay with as small gap as possible (e.g., between 2- and 3-μm gap with roughly 15-dB contrast, but only 1-μm actuated length is needed.)

Fig. 6 shows the simulated surface current and electric-field distribution in one metamolecule with 4-μm gap distance at its Fano resonance frequency of 1.57 THz. One observes a very strong antiparallel currents at the dark mode, which makes the structure weakly coupled to free space, resulting in a narrow dip in transmission spectrum at lower frequency (1.12 THz) on the background of the broad bipolar resonance (bright mode) at much higher frequency. We also notice very high field concentration at the gap between the two elements of the structure, which is responsible for the dramatic resonance shift while changing the gap distance.

Using the analysis of Fano resonances [24], we model the lossless double split ring as an undamped equivalent circuit with a capacitor C_C representing the broadband-bright mode in series with a parallel LC resonance circuit consisting of L_0 and C_0, which simulates the narrowband-dark mode. The stable-input impedance Z of this circuit is

$$Z = -\frac{i}{\omega C_C}\frac{\omega^2\left(\frac{C_C}{C_0}+1\right)-\omega_0^2}{\omega^2-\omega_0^2} \tag{2}$$

where $\omega_0 = \frac{1}{\sqrt{L_0 C_0}}$ is the angular resonance frequency of the dark mode and ω is the angular frequency of interest. The zero of the impedance, which corresponds to the dip in transmission spectrum, is at the frequency

$$\omega = \frac{\omega_0}{\sqrt{\frac{C_C}{C_0}+1}} = \frac{1}{\sqrt{L_0}}\frac{1}{\sqrt{C_0+C_C}}. \tag{3}$$

Because the increased gap capacitance leads to lowering of the Fano resonance Q-factor, we associate the gap capacitance to the bright mode capacitor, or $C_C = C_{C0} + A/x$, where C_{C0} is the lumped bright mode capacitance without the gap, A is a factor associated with the two gap capacitances, and x is the gap distance. From (3), we can see that the relationship between resonance frequency and gap capacitance follows:

$$f = \frac{\omega}{2\pi} = a\frac{1}{\sqrt{b+\frac{1}{x}}} \tag{4}$$

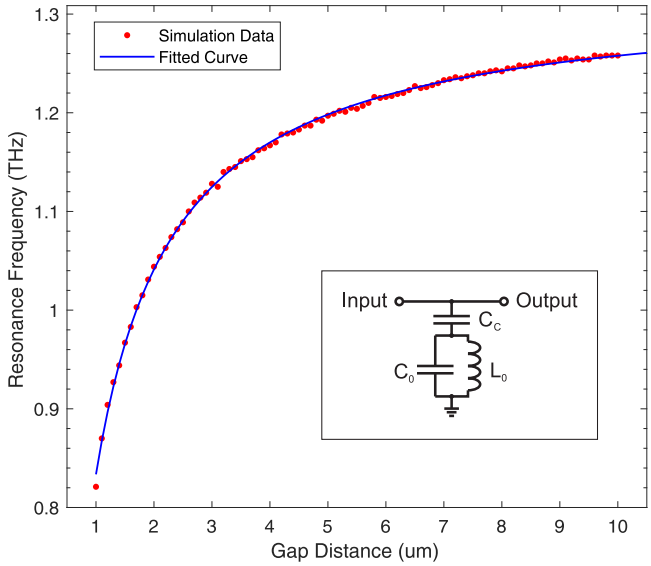

Fig. 7. Simulated resonance frequency position and fitted function. Inset shows the equivalent circuit of the double split-ring Fano resonance without damping. The capacitor C_C represents the broadband-bright mode in coupling with the narrowband-dark mode that consists of parallel L_0 and C_0. The form and numerical values of fit function are discussed in text.

where f is the resonance frequency in THz, x is the gap distance in μm, a and b are the fit factors, and $b \cdot x$ is the ratio between the static capacitance $C_0 + C_{C0}$ and the gap capacitances. The fitting result is shown in Fig. 7, with $a = 1.19$ and $b = 0.79$. We can infer that the gap capacitance in case of 1-μm gap distance accounts for more than 50% of the total bright mode capacitance.

B. Measurement Data and Discussion

For data processing, we select only the part of the measured THz-TDS pulse before the first reflection from the detector crystal. With a signal length around 12 ps, we have about 80-GHz resolution. To better resolve the resonance peak, we use zero padding to interpolate the peak position. TDS transmission spectra for different gap distances are shown in Fig. 8. When normalized to a glass sample, we observe very low insertion loss, less than 1 dB, from the metamaterial itself, as predicted from a simulation result. The 3-dB loss of a glass substrate determined from the reference measurement without a sample is mainly Fresnel reflection loss (11% per air/glass interface) and is much lower than in systems using silicon substrates because of lower refractive index of fused silica in the 0.5- to 2-THz region ($n_{\text{fused silica}} \approx 2$ versus $n_{\text{silicon}} \approx 3.4$ [25]).

The absolute experimental resonance positions are slightly different from simulation values due to uncertainty of model parameters, but when we consider the resonance frequency shift as a function of gap distance, as shown in Fig. 9, the measured and simulated results agree very well with each other. The MDs and Q-factors are lower than the simulated values, which use bulk conductivity at subterahertz frequency for gold. One would anticipate this behavior since the real system will have additional losses compared to the ideal scenario. Fig. 10(a) shows the simulation result when the metal conductivity is only 1/10 of

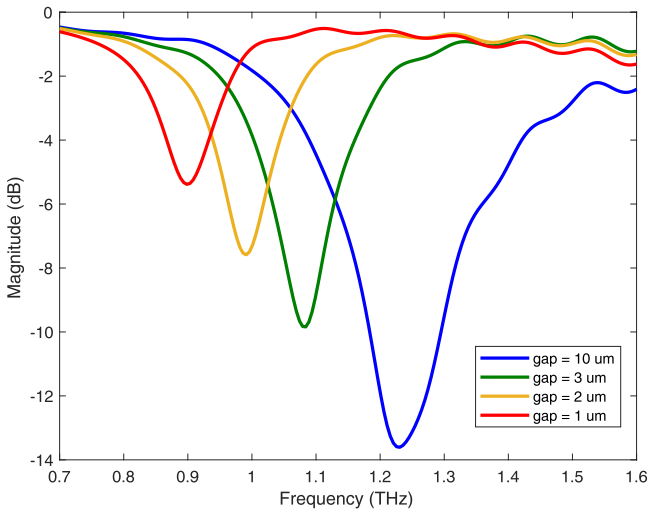

Fig. 8. Measured transmission spectra for different gap distances, normalized to glass sample. The resonance frequency for gap of 1, 2, 3, and 10 μm is 0.9, 0.99, 1.08, and 1.23 THz, respectively.

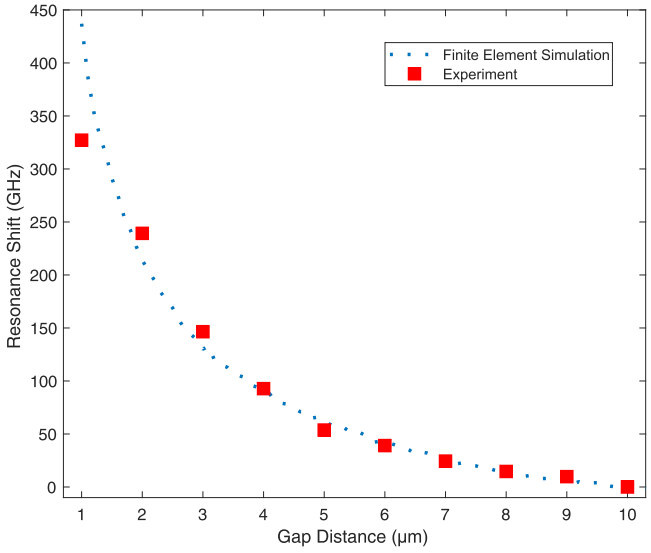

Fig. 9. Measured resonance frequency shift relative to resonance position of 10-μm gap distance. Overlaid dash line is the simulated result. Except for the 1-μm gap distance, all other experimental shifts agree very well with the simulation model.

this value: the resonance is heavily damped and both MD and Q-factor are decreased substantially. The fabricated structure with 100-nm gold film has clearly lower conductivity than that of bulk gold [26], which leads to a resonance with a magnitude between the two extreme cases. For improvement, thicker gold films can be deposited and the chromium layer can be reduced to increase the effective conductivity, which poses no difficulty to the microfabrication process. The dielectric losses of the substrate have a negligible influence and has been incorporated in the simulation model.

Some of the most important properties of a modulator are the MD, operating frequency, percentage of resonance shift, and insertion loss. For MD, because of many different definitions that lead to different values, we use here the standard definition

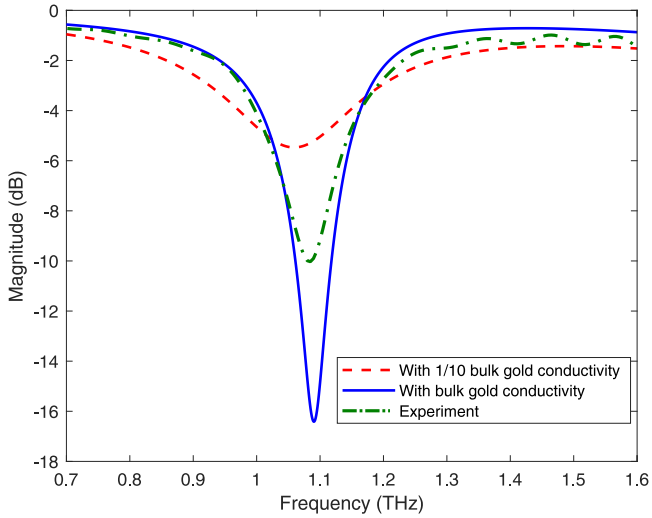

Fig. 10. Simulated spectra with different metal conductivity: bulk gold (41×10^6 S/m) and 1/10 of the bulk conductivity. Superimposed is the experimental spectrum of the structure at the same 3-μm gap distance.

of it as follows:

$$\mathrm{MD} = \frac{I_{\max} - I_{\min}}{I_{\max}} \times 100\% \tag{5}$$

where $I_{\max}$ and $I_{\min}$ are maximum and minimum intensity values, respectively. For engineering purpose, it is more adequate to use log scale for the resonance strength and the depth of modulation can be computed as

$$\mathrm{MD_{dB}} = 10 \times \frac{I_{\max}}{I_{\min}}(\mathrm{dB}). \tag{6}$$

Table I summarizes these properties of the recent modulator proposals. In comparison with the state-of-the-art designs, our sample shows a profound resonance shift of 330 GHz or 35% for the total 9-μm actuated distance. At 1.23 THz, the contrast between the lowest and the highest transmission values, corresponding to 10- and 1-μm separation, respectively, is 13 dB. The MD of the sample is calculated to be 95%, among the highest value of the state-of-the-art modulator demonstrators. Another important characteristic for practical applications is the insertion loss since emitter power is a premium for the terahertz frequency range. Many publications report only the normalized transmission spectra. The loss of the reference substrate of more than 3 dB from reflection alone from Si or GaAs substrates is typically neglected [25], [35]. In our case, the total insertion loss of the as-fabricated structure is only 4 dB, which can be lowered by applying antireflection structures on the back sides [36], since the intrinsic loss of the metamaterial is less than 1 dB.

For fast modulation, it is desired to have low actuation amplitude, and in our case, a proper figure of merit would be the MD or resonance shift per μm actuation. In this respect, the sample shows a maximum of 76% MD and 93-GHz resonance shift per μm. These very high values enable the demonstrated sample to be used as a bandpass filter or a terahertz chopper when coupled with a piezoelectric actuator. Alternatively, the structure could also be converted into an MEM design to enable addressing at

TABLE I
COMPARISON BETWEEN THE STATE-OF-THE-ART THZ MODULATORS

Method	Material	Modulation Depth	Operating Freq.	Freq. Shift[a]	Insertion Loss[b]	Ref.
HEMT	GaAs/AlGaAs	3% / 0.13 dB	0.1-2 THz	-	-	[27]
Schottky	Metal/GaAs	30% / 1.5 dB	0.72 THz	-	>4 dB	[10]
Schottky	Metal/GaAs	52% / 3.2 dB	0.75 THz	-	>14 dB	[28]
Schottky	Metal/GaAs	36% / 1.9 dB	0.63 THz	-	10 dB	[29]
Schottky	Metal/GaAs	50% / 3 dB	-	-	-	[30]
HEMT	Metal/GaAs	30% / 1.5 dB	0.46 THz	-	15 dB	[31]
Graphene	Graphene/Si	15% / 0.7 dB	0.57-0.63 THz	-	>0.2 dB	[32]
MEMS	Metal/SOI	-	0.98 THz	31%	-	[13]
LC	LC/Polyimide	30% / 1.5 dB	2.62 THz	4%	-	[12]
Graphene	Graphene/Si	50% / 3 dB	0.4 THz	-	-	[33]
MEMS	Metal/SiO2	98% / 16.5 dB	0.48 THz	45%	2 dB	[14]
HEMT	Metal/GaAs	80% / 7 dB	0.86 THz	-	7 dB	[34]
Our result	Metal/SiO2	95% / 13 dB	1.23 THz	35%	4 dB	-

[a]Relative to operating frequency.
[b]Loss compared to measurement without sample. Results referenced to substrate measurement are marked with >.

pixel level. Other aspect is the size of a unit cell compared with the working wavelength. Since the materials are fused silica and air, the effective refractive index inside the structure lies between 1 and 2. Hence, the unit cell size, which corresponds to the smallest pixel size in a focal plane array configuration, would be 1/3 to 1/6 of the radiation wavelength inside the metamaterial. The subwavelength pixel size will enable diffraction techniques to be applied to THz beam.

IV. CONCLUSION

We proposed and experimentally demonstrated a modulator-based on the Fano resonance of a vertical asymmetric split-ring structure working in the terahertz frequency range. We achieved 95% MD and 35% resonance frequency tunability at 1.23 THz with less than 1-dB inherent loss. The design shows great potential for realizing high contrast terahertz spatial and temporal modulators for imaging applications.

ACKNOWLEDGMENT

The authors would like to thank the microanalytics and nanoanalytics facility center for the SEM images. The authors would also like to thank all members of their research group for constructive discussions, and especially Dr. R. Bornemann for confocal microscope measurements.

REFERENCES

[1] J. B. Pendry, "Negative refraction makes a perfect lens," *Phys. Rev. Lett.*, vol. 85, no. 18, pp. 3966–3969, 2000.
[2] N. Engheta and R. W. Ziolkowski, *Metamaterials: Physics and Engineering Explorations*. Hoboken, NJ, USA: Wiley, 2006.
[3] N. I. Zheludev and Y. S. Kivshar, "From metamaterials to metadevices," *Nature Mater.*, vol. 11, no. 11, pp. 917–924, 2012.
[4] C. L. Holloway *et al.*, "An overview of the theory and applications of metasurfaces: The two-dimensional equivalents of metamaterials," *IEEE Antennas Propag. Mag.*, vol. 54, no. 2, pp. 10–35, Apr. 2012.
[5] H.-T. Chen, A. J. Taylor, and N. Yu, "A review of metasurfaces: Physics and applications," *Rep. Prog. Phys.*, vol. 79, no. 7, 2016, Art. no. 076401.
[6] H.-T. Chen, J. F. O'Hara, A. K. Azad, and A. J. Taylor, "Manipulation of terahertz radiation using metamaterials," *Laser Photon. Rev.*, vol. 5, no. 4, pp. 513–533, 2011.
[7] B. Reinhard, O. Paul, and M. Rahm, "Metamaterial-based photonic devices for terahertz technology," *IEEE J. Sel. Topics Quantum Electron.*, vol. 19, no. 1, Jan./Feb. 2013, Art. no. 8500912.
[8] X. C. Tong, *Terahertz Metamaterials and Metadevices*. New York, NY, USA: Springer, 2018, pp. 57–70.
[9] M. Rahm, J.-S. Li, and W. J. Padilla, "THz wave modulators: a brief review on different modulation techniques," *J. Infrared, Millimeter, THz Waves*, vol. 34, no. 1, pp. 1–27, 2013.
[10] H.-T. Chen *et al.*, "Active terahertz metamaterial devices," *Nature*, vol. 444, no. 7119, pp. 597–600, 2006.
[11] H.-T. Chen *et al.*, "A metamaterial solid-state terahertz phase modulator," *Nature Photon.*, vol. 3, no. 3, pp. 148–151, 2009.
[12] D. Shrekenhamer, W.-C. Chen, and W. J. Padilla, "Liquid crystal tunable metamaterial absorber," *Phys. Rev. Lett.*, vol. 110, no. 17, 2013, Art. no. 177403.
[13] Y. H. Fu *et al.*, "A micromachined reconfigurable metamaterial via reconfiguration of asymmetric split-ring resonators," *Adv. Functional Mater.*, vol. 21, no. 18, pp. 3589–3594, 2011.
[14] Z. Han, K. Kohno, H. Fujita, K. Hirakawa, and H. Toshiyoshi, "MEMS reconfigurable metamaterial for terahertz switchable filter and modulator," *Opt. Express*, vol. 22, no. 18, pp. 21326–21339, 2014.
[15] U. Fano, "Effects of configuration interaction on intensities and phase shifts," *Phys. Rev.*, vol. 124, no. 6, pp. 1866–1878, 1961.
[16] B. Luk'yanchuk *et al.*, "The fano resonance in plasmonic nanostructures and metamaterials," *Nature Mater.*, vol. 9, no. 9, pp. 707–715, 2010.
[17] B. Gallinet and O. J. Martin, "Ab initio theory of fano resonances in plasmonic nanostructures and metamaterials," *Phys. Rev. B, Condens. Matter*, vol. 83, no. 23, 2011, Art. no. 235427.
[18] N. Papasimakis, V. A. Fedotov, Y. H. Fu, D. P. Tsai, and N. I. Zheludev, "Coherent and incoherent metamaterials and order-disorder transitions," *Phys. Rev. B, Condens. Matter*, vol. 80, no. 4, 2009, Art. no. 041102.
[19] C. Debus and P. H. Bolívar, "Terahertz biosensors based on double split ring arrays," *Proc. SPIE*, vol. 6987, 2008, Art. no. 69870U.
[20] R. Singh *et al.*, "The fano resonance in symmetry broken terahertz metamaterials," *IEEE Trans. THz Sci. Technol.*, vol. 3, no. 6, pp. 820–826, Nov. 2013.
[21] Y. Todorov, P. Desfonds, C. Belacel, L. Becerra, and C. Sirtori, "Three-dimensional THz lumped-circuit resonators," *Opt. Express*, vol. 23, no. 13, pp. 16838–16845, 2015.
[22] A. E. Siegman, M. Sasnett, and T. Johnston, "Choice of clip levels for beam width measurements using knife-edge techniques," *IEEE J. Quantum Electron.*, vol. 27, no. 4, pp. 1098–1104, Apr. 1991.
[23] L. Cong *et al.*, "Fano resonances in terahertz metasurfaces: a figure of merit optimization," *Adv. Opt. Mater.*, vol. 3, no. 11, pp. 1537–1543, 2015.
[24] B. Lv *et al.*, "Analysis and modeling of fano resonances using equivalent circuit elements," *Sci. Rep.*, vol. 6, 2016, Art. no. 31884.

[25] D. Grischkowsky, S. Keiding, M. Van Exter, and C. Fattinger, "Far-infrared time-domain spectroscopy with terahertz beams of dielectrics and semiconductors," *J. Opt. Soc. Amer. B, Opt. Phys.*, vol. 7, no. 10, pp. 2006–2015, 1990.
[26] N. Laman and D. Grischkowsky, "Terahertz conductivity of thin metal films," *Appl. Phys. Lett.*, vol. 93, no. 5, 2008, Art. no. 051105.
[27] T. Kleine-Ostmann, P. Dawson, K. Pierz, G. Hein, and M. Koch, "Room-temperature operation of an electrically driven terahertz modulator," *Appl. Phys. Lett.*, vol. 84, no. 18, pp. 3555–3557, 2004.
[28] H.-T. Chen *et al.*, "Electronic control of extraordinary terahertz transmission through subwavelength metal hole arrays," *Opt. Express*, vol. 16, no. 11, pp. 7641–7648, 2008.
[29] O. Paul *et al.*, "Polarization-independent active metamaterial for high-frequency terahertz modulation," *Opt. Express*, vol. 17, no. 2, pp. 819–827, 2009.
[30] H.-T. Chen *et al.*, "Hybrid metamaterials enable fast electrical modulation of freely propagating terahertz waves," *Appl. Phys. Lett.*, vol. 93, no. 9, 2008, Art. no. 091117.
[31] D. Shrekenhamer *et al.*, "High speed terahertz modulation from metamaterials with embedded high electron mobility transistors," *Opt. Express*, vol. 19, no. 10, pp. 9968–9975, 2011.
[32] B. Sensale-Rodriguez *et al.*, "Broadband graphene terahertz modulators enabled by intraband transitions," *Nature Commun.*, vol. 3, 2012, Art. no. 780.
[33] W. Gao *et al.*,, "High-contrast terahertz wave modulation by gated graphene enhanced by extraordinary transmission through ring apertures," *Nano Lett.*, vol. 14, no. 3, pp. 1242–1248, 2014.
[34] Z. Zhou, S. Wang, Y. Yu, Y. Chen, and L. Feng, "High performance metamaterials-high electron mobility transistors integrated terahertz modulator," *Opt. Express*, vol. 25, no. 15, pp. 17832–17840, 2017.
[35] E. Hecht, *Optics*, 4th ed. Reading, MA, USA: Addison-Wesley, 2002, pp. 116–120.
[36] H.-T. Chen *et al.*, "Antireflection coating using metamaterials and identification of its mechanism," *Phys. Rev. Lett.*, vol. 105, no. 7, 2010, Art. no. 073901.

Tuan Anh Pham Tran was born in Hanoi, Vietnam, in 1984. He received the B.Sc. degree in engineering physics from the Vietnam National University of Hanoi, Hanoi, Vietnam, in 2007, and the M.Sc. degree in optics and photonics from the Karlsruhe Institute of Technology, Karlsruhe, Germany, in 2014.

From 2008 to 2012, he was a Researcher with the National Centre for Technological Progress, Hanoi, where he was engaged in research on industrial laser systems. In 2015, he joined the Institute for High Frequency and Quantum Electronics, University of Siegen, Siegen, Germany, where he is currently involved in the development of terahertz components and systems.

Peter Haring Bolívar (M'02) was born in Mexico City, Mexico, in 1969. He received the degree in electrical engineering from RWTH Aachen University, Aachen, Germany, in 1992.

From 1992 to 1993, he was the Head of the Rescue Equipment Division, Nautica Diesel Europea, Mexico City. From 1993 to 1996, he was a Scientific Assistant with the Institut für Halbleitertechnik II, RWTH Aachen, where he was involved with conjugated polymers and femtosecond dynamics in semiconductors. From 1997 to 2001, he was the Head of ultrahigh-frequency research with the Institut of Semiconductor Electronics, RWTH Aachen. From 2001 to 2004, he was the Head of research at this institution with activities in the fields of optoelectronics, ultrafast science, ultrahigh frequency devices, optical data storage, and nanotechnology. Since 2004, he has been the Head of the Institute for High Frequency and Quantum Electronics, University of Siegen, Siegen, Germany. In 2008, he additionally became the Vice-Rector for Research of this university. Since 2014, he has been representing all the European universities in the ESIF structured dialogue group of the European Commission. He holds 9 patents, 5 book contributions, and has authored or co-authored more than 100 peer-review publications and more than 150 international conference contributions.